Electrochimica Acta 56 (2011) 5966–5971

Contents lists available at ScienceDirect

Electrochimica Acta

journal homepage: www.elsevier.com/locate/electacta

Pt/C anodic catalysts with controlled morphology for direct dimethyl ether fuel cell: The role of consecutive surface

Fengzhan Si[a,c], Xiumei Chen[a], Liang Liang[a], Chenyang Li[a], Jianhui Liao[a], Changpeng Liu[a], Xinbo Zhang[b,*], Wei Xing[a,**]

[a] State Key Laboratory of Electroanalytical Chemistry, Jilin Province Key Laboratory of Low Carbon Chemical Power, Changchun Institute of Applied Chemistry, Chinese Academy of Sciences, 5625 Renmin Street, Changchun 130022, PR China
[b] State Key Laboratory of Rare Earth Resource Utilization, Changchun Institute of Applied Chemistry, Chinese Academy of Sciences, 5625 Renmin Street, Changchun 130022, PR China
[c] Graduate University of Chinese Academy of Sciences, PR China

ARTICLE INFO

Article history:
Received 7 March 2011
Received in revised form 27 April 2011
Accepted 29 April 2011
Available online 6 May 2011

Keywords:
Electrooxidation
Consecutive surface
Anodic catalyst
Direct dimethyl ether fuel cell
Nanowires

ABSTRACT

Two types of Pt nanowires (NWs)/C catalysts with different aspect ratios and one type of Pt nanoparticles/C catalyst are successfully synthesized, and DME electrochemical performance on different extent consecutive surfaces is investigated. The morphology and crystallization are confirmed with electron microscopes and XRD. The electrochemical tests show that the nanowire catalysts, especially the one with higher aspect ratio, possess higher electrochemical surface areas, higher absorption capacity of DME, higher CO tolerance, higher electron transfer coefficient, and higher activity towards DME electrooxidation than those of the nanoparticle catalyst. The results prove that the consecutive surface favors for direct dimethyl ether fuel cell (DDFC) anodic catalyst, which are contributive to the study of the mechanism of DME electrooxidation on Pt surface and designing an effective catalyst for anodic DDFC.

1. Introduction

Dimethyl ether (DME) as the simplest ether which can be produced from natural gas, coal or biomass, is one of the most promising alternative fuels due to higher energy density, less toxic, less corrosive, and easier to be oxidized completely. For simple molecules fuel cell, DME has less effect on fuel crossover because of its weaker molecular polarity [1,2]; its positive variation of entropy (ΔS), and the reversible energy is higher than 100% [3]. The utilization of DME in fuel cell can be classified to three types: solid oxide fuel cell (SOFC) [4–6], hydrogen production [7–10], and direct dimethyl ether fuel cell (DDFC) [11–13]. DDFC is much more appropriate for a portable power device, for operating at lower temperature and needs no external devices [11]. However, the performance of DDFC is still need to be improved for practical application. The cell operating parameters [12–14], the technology of membrane electrode assemble (MEA) [15], and the design of cell structures [12] are all should be developed, but on the top of the list is the performance of anodic catalyst [3,16–18].

In order to improve the electro-oxidation performance of the catalysts for DME, the mechanism has been investigated by single crystal electrodes [19–21] and in situ measurements [22–24]. It is recognized that DME electro-oxidation is a multi-path reaction, but the adsorption manners (e.g. linearly bonded, and bridge-bonded) and the by-products though the reaction (e.g. formic acid and methanol) are controversial, due to the difference of experimental conditions [1,19–24]. Some reports concentrated on nanocube electrocatalysts with preferential {1 0 0} surfaces demonstrated that dimethyl ether electrooxidation on Pt nanocubes exhibits similar features with bulk Pt single crystal electrode and the orientated nano-structures possess high activity [25]. However, the factor of consecutive surface in nano electrocatalysts has not been enough investigated, which is of importance for the study of the mechanism of DME electrooxidation and designing a catalyst towards DME electro-oxidation with high performance.

The objective of this work is to compare the electrochemical behaviors on nanowire (NW) electrocatalyst with consecutive surfaces and those on nanoparticle (NP) electrocatalysts with lots of dislocations; all the electrocatalysts are carbon supported synthesized by controlling the condition of reaction. Therefore, in this study, the NW samples were prepared in a surfactant-free route, using formic acid as a weak reducing agent at room temperature. For comparison, the NP sample was prepared with the same method expect the temperature was 80 °C. The catalysts were

* Corresponding author. Tel.: +86 431 85262235; fax: +86 431 85262235.
** Corresponding author. Tel.: +86 431 85262223; fax: +86 431 85685653.
E-mail addresses: xbzhang@ciac.jl.cn (X. Zhang), xingwei@ciac.jl.cn (W. Xing).

0013-4686/$ – see front matter © 2011 Elsevier Ltd. All rights reserved.
doi:10.1016/j.electacta.2011.04.106

characterized by the X-ray diffraction, transmission electron microscope and scanning electron microscope, and the electrochemical performance for electro-oxidation of DME was studied.

2. Experimental

2.1. Catalyst preparation

In the carbon supported nanowire catalyst (Pt NWs/XC-72R) synthesis, 15 mg Vulcan XC-72R nanospheres as the support were dispersed in 40.5 mL ultrapure water under ultrasonication condition for 30 min. 6.08 mL H_2PtCl_6 solution (0.02 M) and 3 mL HCOOH were added to the suspension. To ensure the dispersion, another process in ultrasonication was carried out for 30 min. The mixture was then stored at room temperature for 72 h. After the reduction, the products were washed with ultrapure water and dried at room temperature [26,27].

To control the aspect ratio of the Pt nanowires, the compressed support (Vulcan XC-72) was employed, and the catalyst (Pt NWs/XC-72) was synthesized using the same procedure, For comparison, the carbon supported nanoparticle catalyst (Pt NPs/XC-72R) was also prepared. Vulcan XC-72R nanospheres and the same procedure were both used, except the reaction temperature was 80 °C.

All the catalysts synthesized above are with Pt loading 60 wt%.

2.2. Catalyst characterization

The scanning electron microscope (SEM) images were obtained using a field emission scanning electron microscopy instrument (Hitachi S-4800), operating at an accelerating voltage of 10 kV. Specimens for SEM were prepared by dispersing as-prepared product in ethanol by sonicating for about 1 min, and then depositing the suspension onto a piece of ITO glass, attached to a SEM brass stub.

Low- to high-resolution transmission electron microscopy and selected area electron diffraction (SAED) patterns were performed using a FEI Tecnai G2 S-Twin instrument with a field emission gun operating at 200 kV, and images were acquired digitally on a Gatan multipole CCD camera. Specimens for all of these TEM experiments were prepared by dispersing the samples in ethanol, sonicating for 2 min to ensure adequate dispersion, and evaporating one drop of the suspension onto a 300 mesh Cu grid, coated with a lacey carbon film.

XRD measurements were performed on a Rigaku-Dmax 2500 diffractometer with Cu Kα radiation ($\lambda = 0.15405$ nm) from 10° to 90° at a scanning rate of 5°/min. The samples were grinded and flattened in a piece of glass with a hole.

2.3. Electrochemical measurements

Electrochemical measurements were performed in a standard three-electrode cell at room temperature. The working electrode was the thin-film electrode with catalysts. Pt foil and Ag/AgCl were used as the counter and reference electrodes, respectively. All potentials in this report referred to Ag/AgCl. All electrolyte solutions were deaerated with high-purity nitrogen for at least 20 min prior to any measurement. Electrode potential was controlled by an EG&G (model 273) potentiostat/galvanostat system.

The working electrode was prepared as follows. First, 5 mg of the catalyst was dispersed in diluted Nafion alcohol solution which contained 1000 μL ethanol and 50 μL Nafion solution (Aldrich, 5 wt% Nafion), and was sonicated for 30 min to obtain a uniform suspension. Second, 10 μL of the suspension was pipetted onto the flat glassy carbon electrode. The coated electrode was then dried at room temperature for 30 min. The glassy carbon electrode was polished with alumina slurry of 0.5 and 0.03 μm successively before use.

All electrochemical measurements were carried out in a 0.5 M $HClO_4$ solution with or without saturated DME (purged into the 0.5 M $HClO_4$ solution for 20 min), and the solutions were deaerated by pure nitrogen for 15 min prior to any measurements without DME. For the electrooxidation of DME, the potential range was from −0.2 to +1.0 V, and for further study, the cyclic voltammetry (CV) at different scan rates were operated. The CO_{ad} stripping voltammograms were measured in a 0.5 M $HClO_4$ solution. CO was purged into the 0.5 M $HClO_4$ solution for 20 min to allow the complete adsorption of CO onto the catalyst when the working electrode was kept at 0.12 mV vs. Ag/AgCl electrode (at the potential of the double-layer), and excess CO in the electrolyte was purged out with N_2 for 30 min. The amount of CO_{ad} was evaluated by integration of the CO_{ad} stripping peak. All the measurements were carried out at room temperature and the stable results were reported. In order to further evaluate the properties of the catalyst, the DME_{ad} stripping voltammograms of the catalyst were tested in the same way as CO_{ad} stripping voltammograms except the working electrode was kept at 0 mV vs. Ag/AgCl electrode when DME was purged into the 0.5 M $HClO_4$ solution for 20 min.

3. Results and discussion

Fig. 1 shows the SEM and TEM images of the three catalysts with the same Pt loading and different nano-structures. From (a) and (c), the samples synthesized at room temperature are carbon nanoshperes covered with Pt nanowires, but the nanowires grown on Vulcan XC-72R are much longer (about 100 nm) than those on Vulcan XC-72 (about 50 nm), for the limited growth space, which are consistent with the results from the TEM images (b) and (d). The SEAD pattern ((b) and (d) insets) shows several bright concentric rings assignable to {1 1 1}, {2 0 0}, {2 2 0}, and {3 1 1} crystal planes of fcc Pt, indicating that the obtained Pt NWs are crystallized in a phase similar to bulk Pt, which is consistent with the X-ray diffraction (XRD) results (Fig. 2). And observed from (e), (f) and insert of (f), the Pt nanoparticle sizes in Pt NPs/XC-72R catalyst are primarily distributed within the range of 3–5 nm, but some of the Pt nanoparticles are severely aggregated.

Fig. 2 shows XRD patterns of Pt NWs/XC-72R (a), Pt NWs/XC-72 (b), and Pt NPs/XC-72R (c) catalysts. The diffraction peaks observed in the three catalysts corresponded to the face-centered cubic phase (fcc) of Pt, and the peaks corresponding to the Pt (1 1 1), Pt (2 0 0), Pt (2 2 0), and Pt (3 1 1) planes are signed in Fig. 2.

From the results of catalyst characterizations, we can define that Pt nano-structures in the three Pt/C catalysts from the controlled synthesis are all crystallized similar as bulk Pt; the anisotropic nanowire structures with different aspect ratios encircled different extents of consecutive surfaces, comparing with the isotropic nano-structures surrounded by little. The objective of comparing catalysts synthesized is to study the role of nano scale consecutive surface in Pt/C DME electrooxidation.

Fig. 3 shows the cyclic voltammograms (CVs) of Pt NWs/XC-72R (a), Pt NWs/XC-72 (b), and Pt NPs/XC-72R (c) in 0.5 M $HClO_4$ solution. Compared with the NP nano-structure catalyst, the NW nanostructure catalysts, especially Pt NWs/XC-72R with higher aspect ratio, possess larger areas of the hydrogen adsorption/desorption peaks, which confirms the larger electrochemical surface area (ECSA) of the NW catalysts. Furthermore, the potential values of the hydrogen desorption peaks for the NW nanostructure catalysts are much more negative than that of the NP nano-structure catalyst, indicating that the

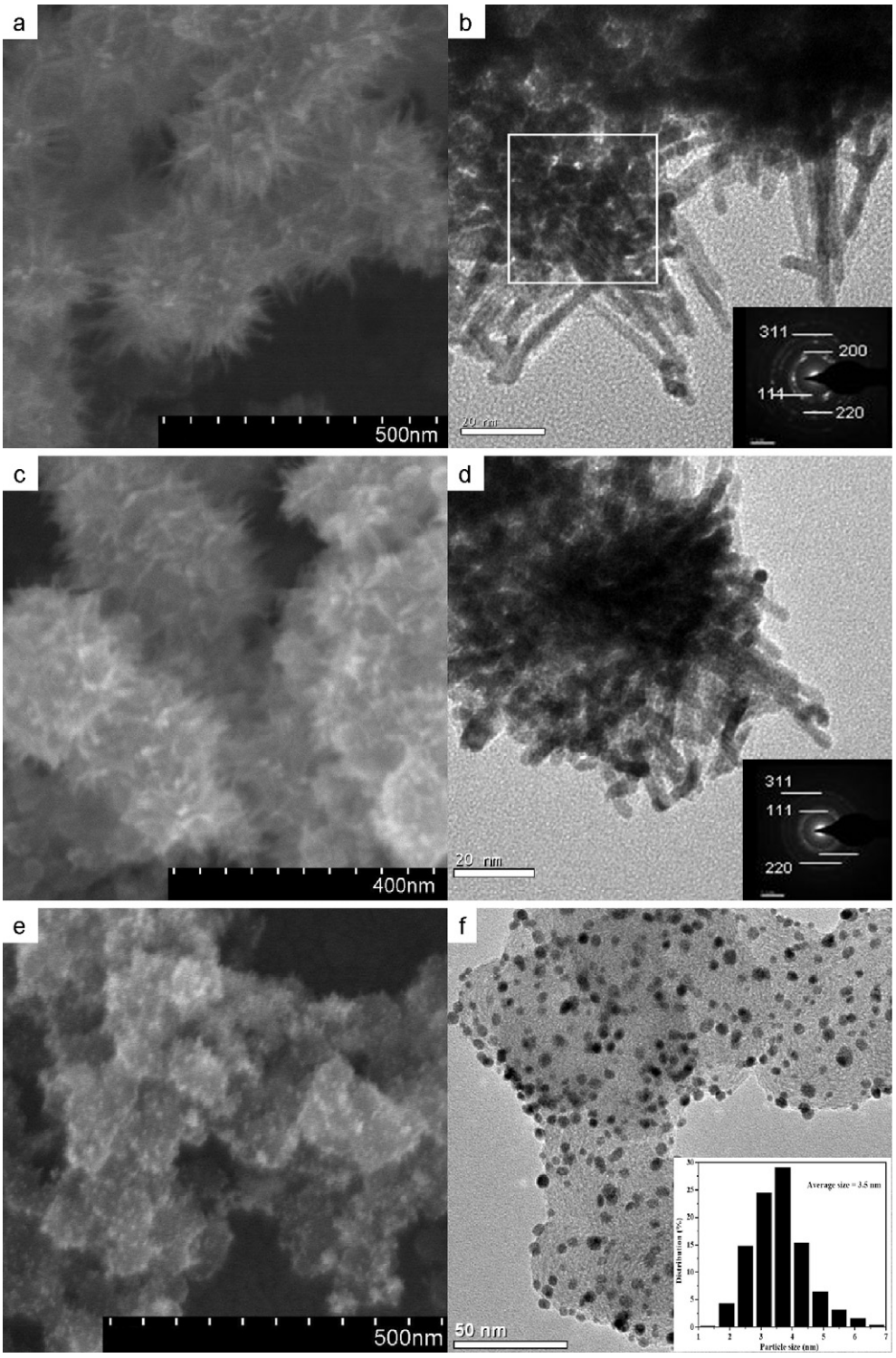

Fig. 1. SEM images of Pt NWs/XC-72R (a), Pt NWs/XC-72 (c), and Pt NPs/XC-72R (e); TEM micrographs of Pt NWs/XC-72R (b), Pt NWs/XC-72 (d), and Pt NPs/XC-72R (f); the inset in (b) and (d): the corresponding SEAD, respectively; the inset in (f): the size distribution histogram of the Pt NPs/XC-72R catalyst.

adsorption strength of hydrogen on the Pt surface is weakened, which is opportune for fuel cell anodic catalysts [28].

The CO_{ad} stripping method was also applied to evaluate the ECSA quantitatively and the CO tolerance of the catalysts. As Fig. 4 shows, the oxidation peaks of CO are shifted negatively about 50 mV on the NW catalysts comparing with the NP sample, suggesting that the NW nano-structure has a capacity of CO tolerance. It is evident that the stripping peak areas at the NW catalyst are much larger than that of the NP catalyst, indicating that there are much more active surface sites on the NW catalyst. Furthermore, the ECSA for the catalyst is calculated by using the CO_{ad} oxidation charge after subtracting the background current. It is 73.09, 52.48 and 49.94 $m^2\ g_{Pt}{}^{-1}$ for Pt NWs/XC-72R, Pt NWs/XC-72, and Pt NPs/XC-72R, respectively. The ECSA of the catalyst is ordered as Pt NWs/XC-72R > Pt NWs/XC-72 > Pt NPs/XC-72R. This result is consistent with those obtained by the hydrogen stripping method.

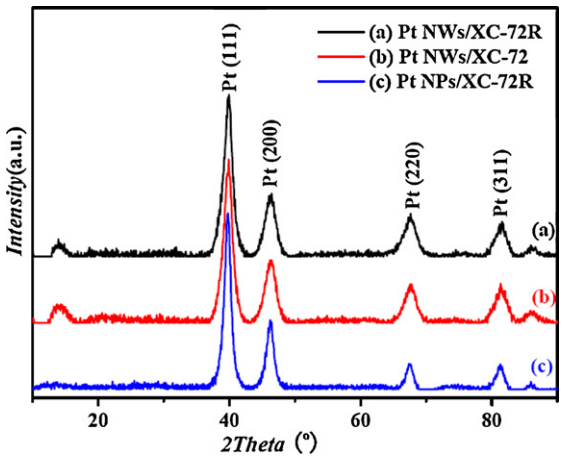

Fig. 2. X-ray diffraction patterns of Pt NWs/XC-72R (a), Pt NWs/XC-72 (b), and Pt NPs/XC-72R (c).

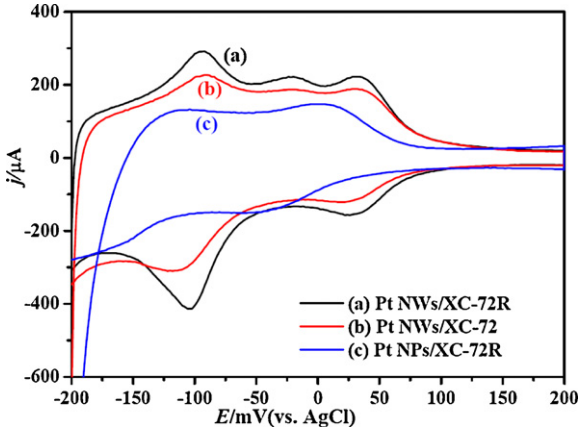

Fig. 3. Cyclic voltammograms (CVs) of Pt NWs/XC-72R (a), Pt NWs/XC-72 (b), and Pt NPs/XC-72R (c) in 0.5 M $HClO_4$ at a scan rate of 20 mV s^{-1}.

Fig. 5 displays the CVs for the electrooxidation of DME in 0.5 M $HClO_4$ solution saturated DME at a scan rate of 25 mV s^{-1}. The double-layer region shows obviously faradaic characteristics during both the positive and negative sweep, which confirms that adsorbed DME species existed on the platinum surface. The electro-oxidation activity of the catalysts for DME is ordered as Pt NWs/XC-72R > Pt NWs/XC-72 > Pt NPs/XC-72R, according to the oxidation current. The order of the electro-oxidation activity is consistent with the order of ECSA. The peak of the NP sample is boarder than that of the NW samples, and the NW sample with the lower aspect ratio corresponding to the boarder peak. These phenomena indicate that either different platinum sites has to be considered for DME oxidation, or that different DME oxidation mechanisms take place [23]. The ratio of the positive peak oxidation current density (I_p) to the negative peak current density (I_n), used to describe the catalyst tolerance to the accumulation of carbonaceous species [17], is higher as the aspect ratio higher, which is consistent with the results of CO_{ad} stripping.

The CVs of the Pt/C catalysts in 0.5 M $HClO_4$ solution saturated DME are shown in Fig. 6 with different scan rates of 5, 10, 20, 50, and 75 mV s^{-1} for Pt NWs/XC-72R, Pt NWs/XC-72, and Pt NPs/XC-72R. The peak potentials shift in positive direction with scan rate, indicating the oxidation of DME is an irreversible charge transfer process [17]. For comparison, the curves of the peak current vs. the square root of scan rates of the CVs are in (d). The linear relationship is attributed to a diffusion controlled process. The relation-ship

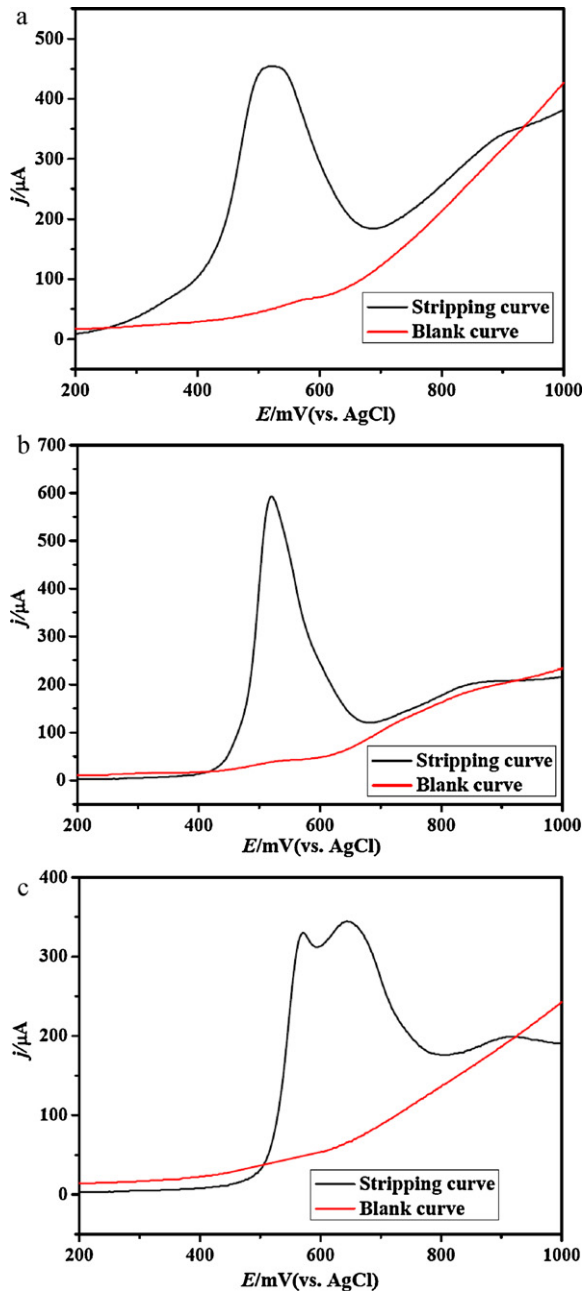

Fig. 4. CO_{ad} stripping voltammograms of Pt NWs/XC-72R (a), Pt NWs/XC-72 (b), and Pt NPs/XC-72R (c) in 0.5 M $HClO_4$ at a scan rate of 20 mV s^{-1}.

between the peak current and the square root of scan rates complies with the following equation:

$$i_p = 2.99 \times 10^5 n(\alpha n')^{1/2} A C_\infty D_0^{1/2} \upsilon^{1/2+} \quad (1)$$

where I_p is the peak current, n is the electron-number for the total reaction, n' is the electron-number transferred in the rate-determining step, α is the electron transfer coefficient of the rate-determining step, A is the electrode surface area, C_∞ is the bulk concentration of the reactant, D_0 is the diffusion coefficient, υ is the potential scan rate. In this paper, the slope of the i_p vs. the square scan rate is $2.99 \times 10^5 n(\alpha n')^{1/2} C_\infty D_0{}^{1/2} \upsilon^{1/2}$. In the same electrolyte and the same reaction, the parameters n, C_∞ and D_0 are constant; therefore, the slope is decided by $\alpha n'$. The corresponding slope for Pt NWs/XC-72R, Pt NWs/XC-72, and Pt NPs/XC-72R is 8.588, 6.599, and 3.212, respectively. The electron transfer coefficient of Pt NWs/XC-72R is 167.4% higher than that of Pt NPs/XC-72R,

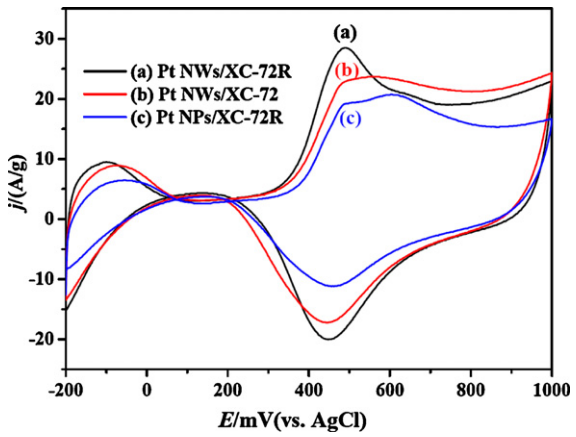

Fig. 5. Cyclic voltammograms of the electrooxidation of DME in 0.5 M $HClO_4$ solution saturated DME for Pt NWs/XC-72R (a), Pt NWs/XC-72 (b), and Pt NPs/XC-72R (c) at a scan rate of 25 mV s^{-1}.

105.4% higher than that of Pt NWs/XC-72. It can be concluded that the NW nano-structure with larger consecutive surface favor for the DME electrooxidation.

Fig. 7 shows DME_{ad} stripping voltammograms of Pt NWs/XC-72R (a), Pt NWs/XC-72 (b), and Pt NPs/XC-72R (c) in 0.5 M $HClO_4$ at a scan rate of 20 mV s^{-1}. The electrooxidation peak potentials of the NW samples are 80 mV more negative than that of the NP sample, consistent with the CO electrooxidation peak currents from CO_{ad} stripping. And the area of the electrooxidation peaks

Table 1
Q_H° and Q_H concluded from Fig. 7 and coverage, θ_{org} concluded as Eq. (2).

	Q_H° (μA mV)	Q_H (μA mV)	θ_{org}
Pt NWs/XC-72R	13,843	2031	0.853
Pt NWs/XC-72	15,569	2710	0.826
Pt NPs/XC-72R	8332	1784	0.786

is 28,462, 26,954, and 19,187 μA mV, respectively, indicating that the catalytic activity of NW nano-structure. To further investigate the adsorption capacity of different catalysts, the coverage (θ_{org}) with DME species is calculated (Table 1) as the following equation [29]:

$$\theta_{org} = \frac{Q_H^\circ - Q_H}{Q_H^\circ} \quad (2)$$

Q_H° is the quantity of electricity related to the adsorption of hydrogen in the supporting electrode (0.5 M $HClO_4$) alone, and Q_H is the same quantity, but in the presence of DME. The results (Table 1) can be concluded that the NW nano-structure with higher aspect radio possesses the highest θ_{org}, and the NP sample corresponding to the lowest one, which prove the larger adsorption capacity of DME on NW nano-structure with extended consecutive surface.

The results above show that the NW nano-structure, especially the one with high aspect ratio, favors for DME electrooxidation, because of the consecutive surface rich catalysts have advantages on ECSA, CO tolerance, and absorption capacity of DME.

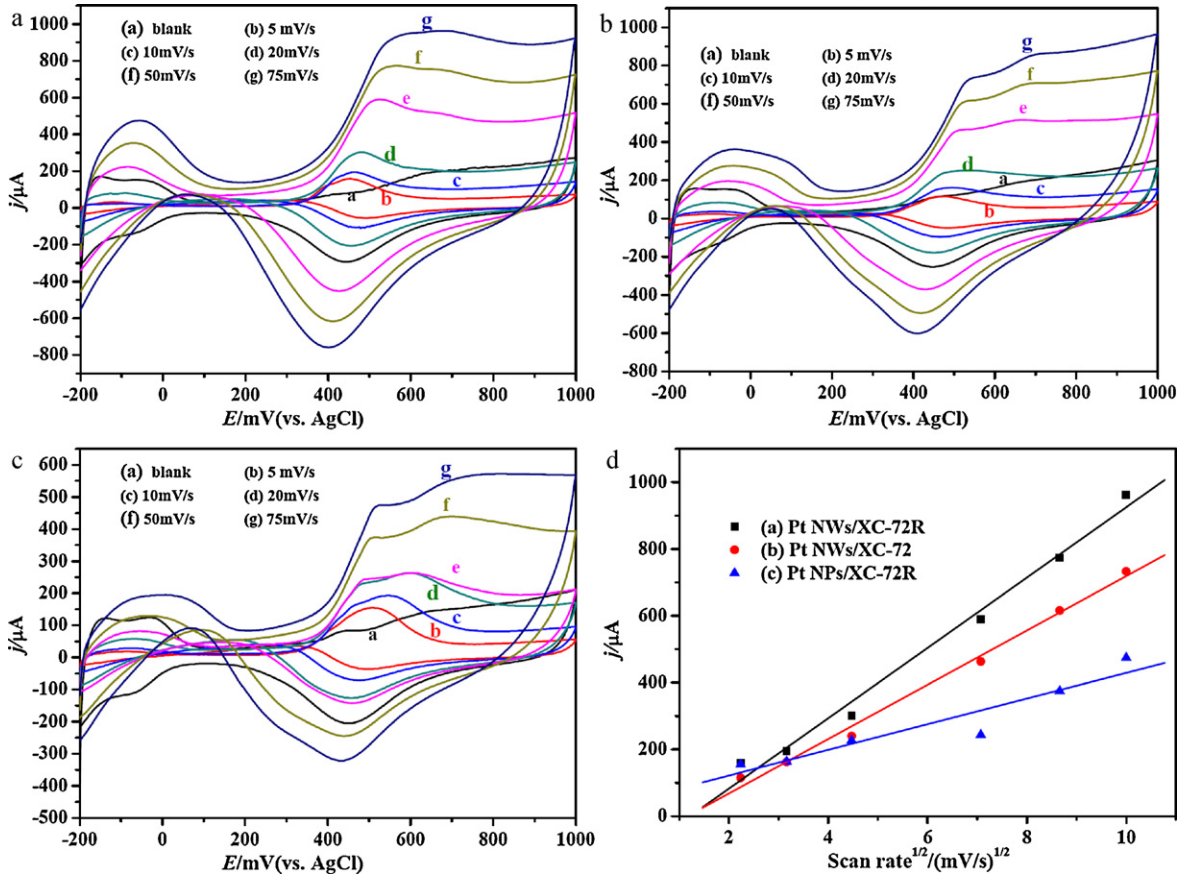

Fig. 6. CVs of the catalysts Pt NWs/XC-72R (a), Pt NWs/XC-72 (b), and Pt NPs/XC-72R (c) in 0.5 M $HClO_4$ solution saturated DME with different scan rates of 5, 10, 20, 50, and 75 mV s^{-1}, and the curves of blank were obtained in 0.5 M $HClO_4$ solution without DME at a scan rate of 25 mV s^{-1}. (d) The linear relationships between the peak currents and the square roots of the scan rates.

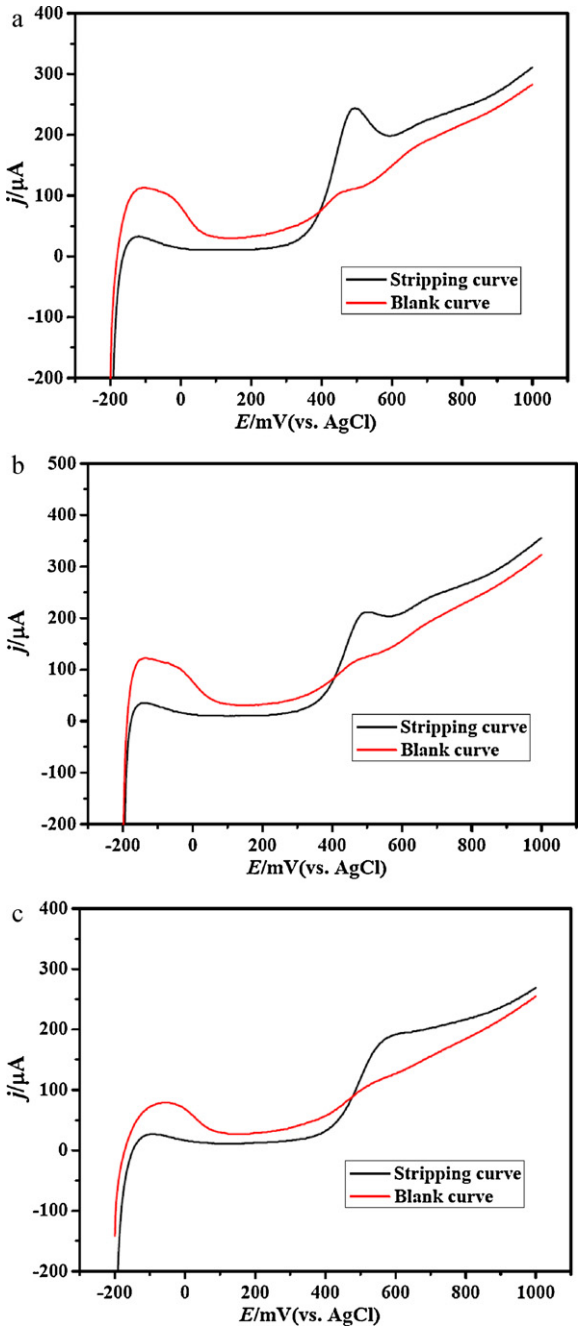

Fig. 7. DME_{ad} stripping voltammograms of Pt NWs/XC-72R (a), Pt NWs/XC-72 (b), and Pt NPs/XC-72R (c) in 0.5 M $HClO_4$ at a scan rate of 20 mV s^{-1}.

4. Conclusion

This study demonstrates that the Pt catalysts with larger consecutive surface have higher performance on DME electrooxidation. The catalysts were synthesized in the same route, and the morphology of the catalysts was nanowires with different aspect ratios and nanoparticles, respectively, which were confirmed by TEM and SEM results. All the Pt nanostructures in catalysts were crystallized as fcc structure as the XRD results. The difference among the Pt catalysts is the extent of consecutive surface. As the investigations on the electrochemical surface area (ECSA), the electrooxidation activity, CO tolerance, adsorption capacity of DME, the consecutive surface is benefit for DME electrooxidation. The results are contributive to the study of the mechanism of DME electrooxidation on Pt surface and to designing an effective catalyst for anodic DDFC.

Acknowledgements

We gratefully thank the reviewers for their valuable suggestions and comments. This work was financially supported by the National Natural Science Foundation of China (20933004, 21011130027, and 21073180), High Technology Research Program of Science and Technology Ministry of China (863 program, 2007AA05Z159, 2007AA05Z143 and 2009AA05Z111), and Jilin Province Science and Technology Development Program (20100102).

References

[1] A. Serov, C. Kwak, Appl. Catal. B 91 (2009) 1.
[2] T.A. Semelsberger, R.L. Borup, H.L. Greene, J. Power Sources 156 (2006) 497.
[3] G. Kerangueven, C. Coutanceau, E. Sibert, J.M. Leger, C. Lamy, J. Power Sources 157 (2006) 318.
[4] E.P. Murray, S.J. Harris, H.W. Jen, J. Electrochem. Soc. 149 (2002) A1127.
[5] E.P. Murray, S.J. Harris, J. Liu, S.A. Barnett, Electrochem. Solid State Lett. 8 (2005) A531.
[6] P. Heo, M. Nagao, M. Sano, T. Hibino, J. Electrochem. Soc. 155 (2008) B92.
[7] T.A. Semelsberger, R.L. Borup, J. Power Sources 155 (2006) 340.
[8] T.A. Semelsberger, R.L. Borup, J. Power Sources 152 (2005) 87.
[9] Q.J. Zhang, X.H. Li, K. Fujimoto, K. Asami, Catal. Lett. 102 (2005) 197.
[10] Q.J. Zhang, X.H. Li, K. Fujimoto, K. Asami, Appl. Catal. A 288 (2005) 169.
[11] M.M. Mench, H.M. Chance, C.Y. Wang, J. Electrochem. Soc. 151 (2004) A144.
[12] K.D. Cai, G.P. Yin, L.L. Lu, Y.Z. Gao, Electrochem. Solid State Lett. 11 (2008) B205.
[13] J.Y. Im, B.S. Kim, H.G. Choi, S.M. Cho, J. Power Sources 179 (2008) 301.
[14] J.H. Yoo, H.G. Choi, C.H. Chung, S.M. Cho, J. Power Sources 163 (2006) 103.
[15] K.D. Cai, G.P. Yin, H. Zhang, Z.B. Wang, C.Y. Du, Y.Z. Gao, Electrochem. Commun. 10 (2008) 238.
[16] T. Haraguchi, Y. Tsutsumi, H. Takagi, N. Tamegai, S. Yamashita, Electr. Eng. Jpn. 150 (2005) 19.
[17] Q. Zhang, Z.F. Li, S.W. Wang, W. Xing, R.J. Yu, X.J. Yu, Electrochim. Acta 53 (2008) 8298.
[18] Y. Liu, S. Mitsushima, K. Ota, N. Kamiya, Electrochim. Acta 51 (2006) 6503.
[19] L.L. Lu, G.P. Yin, Z.B. Wang, K.D. Cai, Y.Z. Gao, Catal. Commun. 10 (2009) 971.
[20] L.L. Lu, G.P. Yin, Y.J. Tong, Y. Zhang, Y.Z. Gao, M. Osawa, S. Ye, J. Electroanal. Chem. 619 (2008) 143.
[21] L.L. Lu, G.P. Yin, Y.J. Tong, Y. Zhang, Y.Z. Gao, M. Osawa, S. Ye, J. Electroanal. Chem. 642 (2010) 82.
[22] Y. Liu, M. Muraoka, S. Mitsushima, K.I. Ota, N. Kamiya, Electrochim. Acta 52 (2007) 5781.
[23] G. Kerangueven, C. Coutanceau, E. Sibert, F. Hahn, J.M. Leger, C. Lamy, J. Appl. Electrochem. 36 (2006) 441.
[24] Y. Zhang, L.L. Lu, Y.J. Tong, M. Osawa, S. Ye, Electrochim. Acta 53 (2008) 6093.
[25] L.L. Lu, G.P. Yin, Z.B. Wang, Y.Z. Gao, Electrochem. Commun. 11 (2009) 1596.
[26] S.H. Sun, F. Jaouen, J.P. Dodelet, Adv. Mater. 20 (2008) 3900.
[27] S.H. Sun, D.Q. Yang, D. Villers, G.X. Zhang, E. Sacher, J.P. Dodelet, Adv. Mater. 20 (2008) 571.
[28] A.C.C. Tseung, K.Y. Chen, Catal. Today 38 (1997) 439.
[29] A. Papoutsis, J.M. Leger, C. Lamy, J. Electroanal. Chem. 234 (1987) 315.